Journal of Materials Science Research and Reviews

Volume 7, Issue 4, Page 641-648, 2024; Article no.JMSRR.124403

Preparation and Properties of Composite Oxide Hydrogen Blocking Coatings by Sintering Method

Yipeng Xie [a], Bo Zhou [a], Feng Wang [a], Yuefeng Wang [a], Pengpeng liu [a], Zaiqiang Feng [b] and Mingqi Tang [b*]

[a] Henan Boiler and Pressure Vessel Inspection Technology Research Institute, Zhengzhou 450016, China.

[b] School of Material Science and Engineering, North China University of Water Resources and Electric Power, Zhengzhou 450045, China.

Authors' contributions

This work was carried out in collaboration among all authors. All authors read and approved the final manuscript.

Article Information

Open Peer Review History:
This journal follows the Advanced Open Peer Review policy. Identity of the Reviewers, Editor(s) and additional Reviewers, peer review comments, different versions of the manuscript, comments of the editors, etc are available here: https://www.sdiarticle5.com/review-history/124403

Original Research Article

Received: 02/08/2024
Accepted: 05/10/2024
Published: 09/10/2024

ABSTRACT

The α-Al_2O_3/Cr_2O_3/SiO_2 composite coating was prepared on a 316L stainless steel sheet using ceramic sintering method. The effect of sintering temperature on the forming of the coating was studied, and the microstructure, thermal shock resistance and electrochemical hydrogen permeation of the coating were observed by XRD, SEM, thermal shock method and electrochemical hydrogen permeation test apparatus. The main research results are as follows: When sintering at 725℃ and slurry ratio is 1:5, the coating surface is uniform, no pores and cracks occur, and the average thickness is about 64μm. The microstructure analysis showed that Cr_2O_3 and SiO_2 were uniformly distributed in the coating, Al_2O_3 segregation existed outside the coating,

**Corresponding author: Email: tangmq400@163.com;*

Cite as: *Xie, Yipeng, Bo Zhou, Feng Wang, Yuefeng Wang, Pengpeng liu, Zaiqiang Feng, and Mingqi Tang. 2024. "Preparation and Properties of Composite Oxide Hydrogen Blocking Coatings by Sintering Method". Journal of Materials Science Research and Reviews 7 (4):641-48. https://journaljmsrr.com/index.php/JMSRR/article/view/356.*

and a new phase of Al_2SiO_5 was produced. Compared to 316L, the coating in slurry ratio 1:5 has best hydrogen stability and thermal shock resistance with permeability reduction factor (PRF) is 15.31. In addition, the composite coating has good thermal shock resistance and can withstand 20 thermal cycles at 450℃.

Keywords: Hydrogen blocking coating; 316L stainless steel; ceramic sintering method; hydrogen blocking performance.

1. INTRODUCTION

As a green and clean secondary energy source, hydrogen energy will play an essential role in the future global energy system [1]. Hydrogen transportation mainly adopts high-pressure gas, low-temperature liquid, and pipeline transportation. Due to the small volume of hydrogen atoms, it is easy to penetrate the metal under a high-pressure environment and cause the deterioration of material properties, such as hydrogen damage, hydrogen brittleness, and other performance problems, which may lead to severe production safety accidents and economic losses. Therefore, the hydrogen energy industry urgently needs to solve the safety problems in the storage and transportation of hydrogen [2,3].

To slow down the penetration and diffusion of hydrogen in metal structural materials, the preparation of hydrogen-blocking coatings was an effective means to prevent or delay the penetration of hydrogen into the material and prevent the occurrence of hydrogen embrittle [4-6]. Traditional ceramic hydrogen blocking coatings can be divided into non-oxide coatings and oxide coatings, such as titanium ceramics such as titanium carbide (TiC), titanium nitride (TiN) and titanium aluminum nitride (TiAlN), silicide ceramics such as silicon carbide (SiC) and silicon nitride (Si_3N_4), oxides ceramic such as aluminium oxide (Al_2O_3), chromic oxide (Cr_2O_3), erbium oxide (Er_2O_3), silicon oxide (SiO_2) and titanium oxide (TiO_2), etc.[7-10]. Compared with silicides, carbides and other coatings, oxide coatings have the advantages of good high temperature resistance and chemical stability, can effectively prevent the penetration of hydrogen, improve the corrosion resistance and safety of metal materials. In particular, Al_2O_3 coating, as a hydrogen resistant coating, has excellent hydrogen resistance and chemical stability, and can effectively protect the metal matrix from the influence of hydrogen embrittlement and corrosion. However, Al_2O_3 coating also has some problems, such as low bonding strength and easy peeling. To solve this problem, Al_2O_3 is generally mixed with gas oxides to make composite coatings [11,12]. The thermal expansion coefficient of Cr_2O_3 is not much different from that of stainless steel, and the binding force of Cr_2O_3 coating is better. It also has excellent hydrogen resistance and chemical stability [13]. However, the coatings fired by these two composite materials have no ceramic luster and poor topography. At the same time, the addition of SiO_2 can be used as the glaze of the ceramic coating to improve the coating topography, and the addition of SiO_2 can optimize the microstructure of the coating and adjust the physical properties of the coating [14,15].

Therefore, α-Al_2O_3, Cr_2O_3, and SiO_2 has been mixed in a particular proportion to make a powder, and a certain amount of binder is expected to have a dense structure and uniform organization of hydrogen-blocking coating. In this paper, α-Al_2O_3/Cr_2O_3/SiO_2 composite oxide hydrogen blocking coating was prepared by optimizing the sintering temperature and slurry ratio. The coating's microstructural morphology, and phase composition were analyzed, and the thermal shock and hydrogen-blocking performance were tested.

2. MATERIALS AND METHODS

316L stainless steel round sheet with a size of Φ32 mm×2 mm was used as the base material of the hydrogen resistance coating. In turn, 400#-1000# SiC sandpaper was used to polish the stainless steel surface. The sample was then cleaned in analytical alcohol using ultrasonic waves. Finally, the sample was placed in the oven at 50℃ for drying.

Firstly, α-Al_2O_3, Cr_2O_3, and SiO_2 with a mass ratio of 1:1:2:6 were weighed by a balance, and ground by a planetary ball mill for 2 h to make the three powders mixed evenly. Secondly, the evenly mixed powder was mixed with inorganic silica gel at a ratio of 1:5, and an evenly dispersed slurry was obtained by mechanical stirring for 1h. Third, the slurry was coated on the

stainless steel matrix by the spinning coating method and dried naturally for 24 hours. Finally, the samples were sintered in Muffle furnace at different temperatures to obtain the hydrogen resistance coating, and the sintering temperature was 2℃/min.

X-ray diffractometer model DX-2700BHX was used for coating phase analysis; the test Angle was 10-90°, the scanning speed was 6°/min, the tube voltage was 40kV, and the tube current was 30mA. Scanning electron microscopy (SEM) model TESCANVEGA3-LMU and its equipped energy spectrometer were used to observe the morphology and composition of the coating surface and cross-section.

The electrochemical hydrogen penetration method was used to test the hydrogen inhibition performance of the coating [16]. The basic principle was to evaluate the barrier effect of the coating on hydrogen diffusion by constructing a two-part system consisting of a cathode pool and an anode pool. NaOH solution was used as the electrolyte in the anode chamber, and the electrolyte in the cathode chamber was a mixed solution of NaOH and thiourea. The specimen was plated with nickel to prevent the diffused hydrogen from recombining into hydrogen molecules. The specimen clamp was placed in the system to ensure the nickel-coated surface faced the anode side. Then, the delay time method [16] was used to calculate the hydrogen permeability coefficient of the sample:

$$D = \frac{L^2}{6t_L} \quad (1)$$

Where D is the apparent hydrogen permeability coefficient, L is the thickness of the sample used, and the hydrogen permeation current is the time subtracted by the time when the hydrogen permeation experiment began. The hydrogen permeability reduction factor PRF was calculated by comparing the permeability coefficient of H ion in the downstream chamber between the uncoated stainless steel matrix and the coated stainless steel sample.

A static thermal shock test was adopted, and the sample was put into the Muffle furnace, held for 450 minutes, and then quenched to observe the morphology changes of the coating and the thermal shock resistance of the coating. The above experiment was repeated until the coating fell off, and the number of thermal shocks was counted.

A static thermal shock test was adopted; and the sample was held for 30 minutes in Muffle furnace and then quenched to make the changes effective. The thermal shock was repeated until the coating failed macroscopically and the number of thermal shocks was counted. The morphology of the coating and the thermal shock resistance of the coating were observed by an optical microscope.

3. RESULTS AND DISCUSSION

3.1 Coating Phase Composition

Fig. 1 shows the XRD pattern of the coating sintered at different temperatures. It can be seen that under the sintering at the above four temperatures, the coating phase was the same, the α-Al_2O_3 phase, the Cr_2O_3 phase, the SiO_2 phase, and the Al_2SiO_5 phase, and no new phase was produced. Under the conditions of the

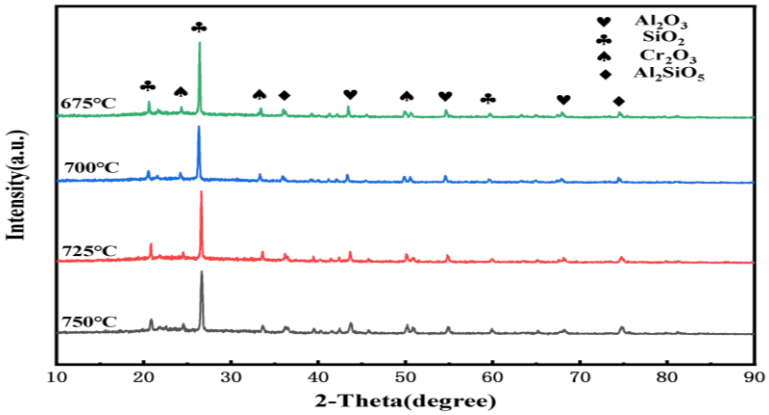

Fig. 1. X-ray diffraction patterns of composite coatings at different sintering temperatures

temperature and slurry ratio, the main phases of the coating were the α-Al_2O_3 phase, Cr_2O_3 phase, SiO_2 phase, and Al_2SiO_5 phase, among which the α-Al_2O_3 phase, Cr_2O_3 phase, and SiO_2 phase were mainly from the added oxide powder. Al2SiO5 was a new phase precipitated by the reaction of the α-Al_2O_3 phase and SiO_2 phase at high temperatures [17].

3.2 Coating Morphology

Fig. 2 shows the macroscopic morphology of the composite coating prepared by sintering. As can be seen in this figure, in sintering temperature 675℃, there were many large pores on the surface of the coating, exposing the stainless steel matrix, and the coating was matte. When the temperature increased to 700℃, the number of pores decreased, the area also decreased, only scattered small pores formed, and the coating surface was smooth. When the temperature was increased to 725℃, the number of pores reached the minimum, the coating surface was smooth, and the coating morphology was best. When the temperature rose to 750 ° C, the coating surface began forming a larger area of pores, a small part of the stainless steel matrix was exposed, and the coating quality decreased. By comparing the surface morphology of the coating at several temperatures, it was found that the coatings sintered at 725°C were homogeneous and had fewer defects, so the sintering temperature of the coating was determined to be 725℃.

The best morphology of composite coating was prepared when the slurry ratio was 1:5, and the sintering temperature was 725℃. To study the microstructure of the coating further, scanning electron microscopy was used to observe the surface and cross-section of the coating. Fig. 3 shows the surface topography of α-Al_2O_3/Cr_2O_3/SiO_2 composite coating at different magnifications. In general, the coating surface was relatively flat, and there were no pores, cracks, or other defects. However, the chosen oxide particle size varied; the oxide particles exhibited agglomeration, and the coating surface displayed slight variations in pits and particles.

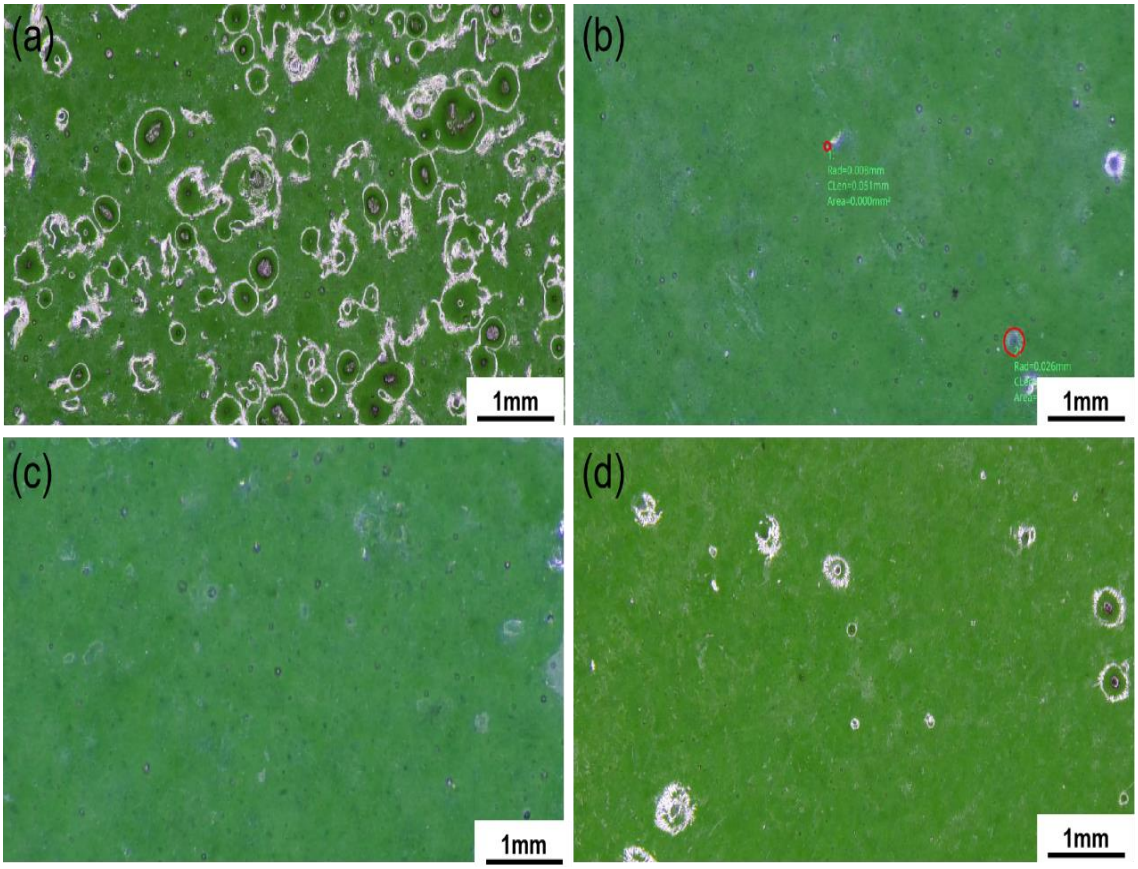

Fig. 2. Macroscopic morphology of sintered coatings at different temperatures: (a)675℃; (b)700 ° C; (c)725 ° C; (d)750℃

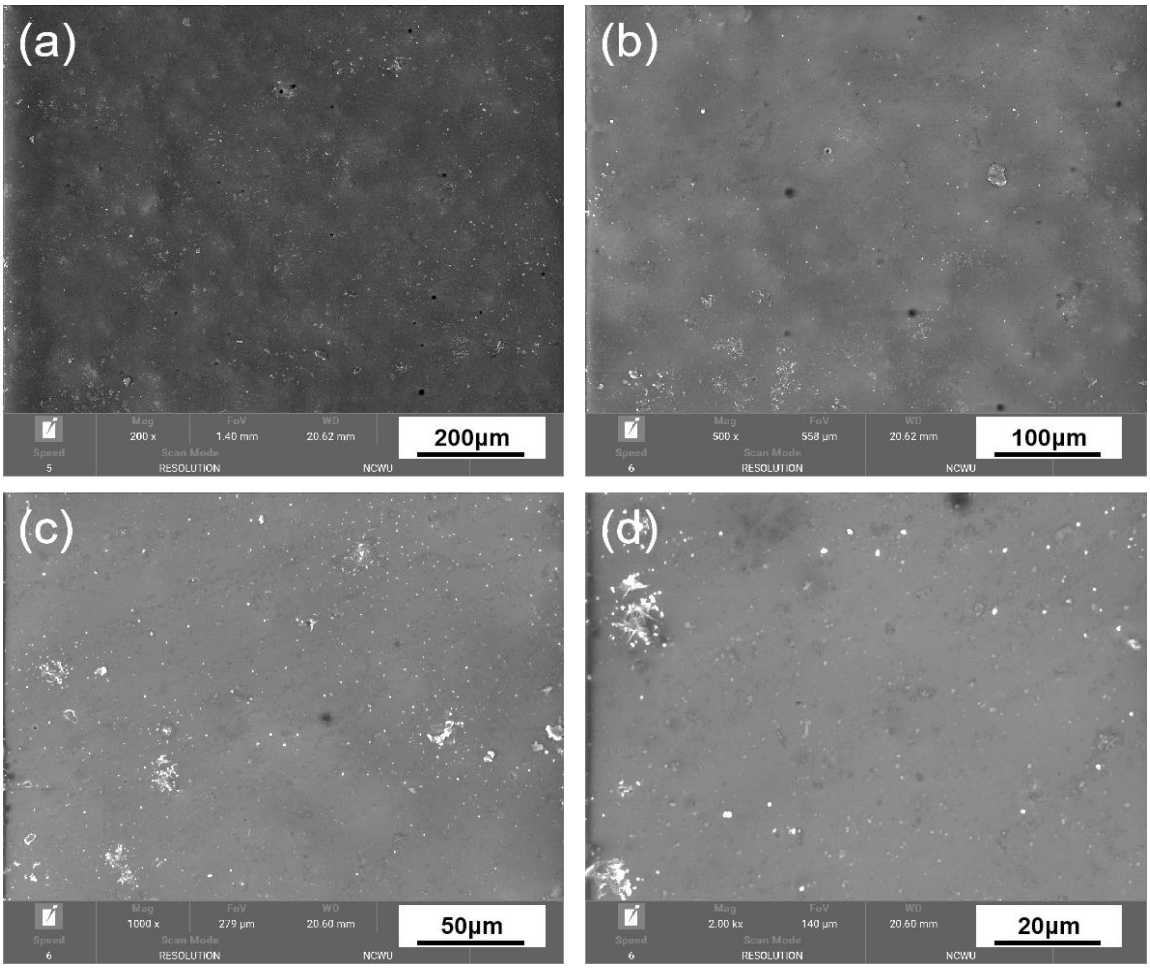

Fig. 3. Surface topography at different magnifications: (a)200x; (b)500x; (c)1000x; (d)2000x

Fig. 4 shows the cross-section topography of the coating. It can be measured that the average thickness of the coating 64 µm with about 15µm pores. This must have occurred because the oxide particle size used in the coating preparation was different; the different particles were stacked together, and there were specific pores, inorganic silica gel adhesive as a liquid phase, filled in these pores so that the particles were combined. Still, carbon and other elements were in the inorganic silica gel adhesive; by increasing the temperature, the elements were oxidized, and other gases, such as CO_2, were generated. When the temperature reached the glass transition temperature (Tg), the components were transformed in liquid phase. Still, the coating surface was sintered faster and became dense, preventing the gas inside the coating from being discharged, resulting in portion gas remaining inside the coating. After the sintering was completed, the undischarged gas formed pores. Although there are pores in the coating, they do not penetrate the entire coating, and no cracks were created around, reducing the risk of coating detachment.

3.3 Hydrogen Resistance Performance

Fig. 5 compare the hydrogen resistance curves of the stainless steel matrix and composite coating at room temperature. According to formula (1), the PRF of the stainless steel matrix and composite coating were calculated to be 1 and 15.3, respectively. One of the reasons for the excellent hydrogen resistance of the coating was the formation of the Al_2SiO_5 (simple cube) crystal structure during the high-temperature sintering process. This crystal structure has high density and stability, making the coating atoms more tightly packed and forming a dense lattice structure with good hydrogen resistance. Secondly, EDS results showed that a large amount of α-Al_2O_3 and Cr_2O_3 were enriched on the surface of the coating. These two oxides have high electronegativity and greater interaction force with oxygen molecules, thus

forming a dense oxide layer on the surface of the coating. In addition, inorganic silica gel was used as an adhesive, SiO_2 was used as a ceramic sinter, and its molecular structure contained a large number of silicon-oxygen bonds, which made a dense layer of silica compounds formed on the surface of the coating, and the hydrogen channel in the coating became smaller, thus increasing the coating barrier to hydrogen.

3.4 Thermal Shock Resistance

Fig.6 shows the coating morphology with a slurry ratio 1:5 before and after test thermal shock at 450℃. After five thermal shocks, the morphology of the coating did not change. After twenty thermal shocks, a large number of black spots and pores appeared in the coating, and the surface topography of the coating became worse, indicating that with the increase in the number of thermal shocks, the coating structure began to be damaged. These defects would become channels for hydrogen penetration. After twenty-five thermal shocks, the black spots in the coating expanded greatly, and the pores became larger; the stainless steel matrix was exposed, the direct contact between the matrix and the external environment could no longer be effectively prevented, and the insulation of the coating to hydrogen was completely lost.

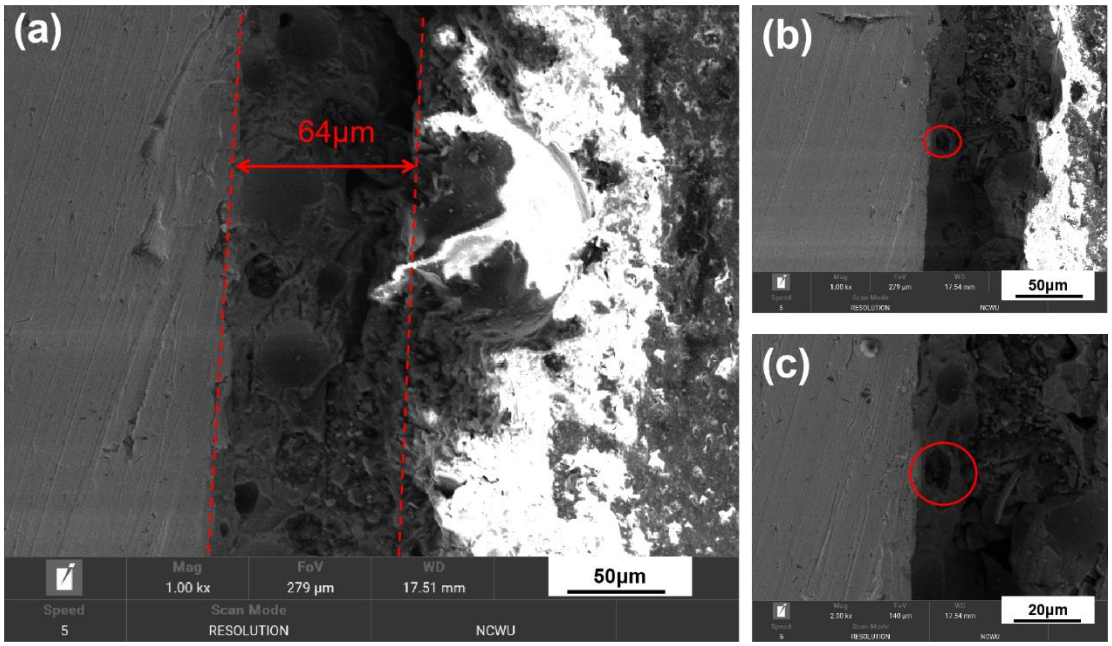

Fig. 4. Coating thickness micrograph and cross-section topography in different magnifications: (a) coating thickness diagram, (b)1000×, (c)2000×

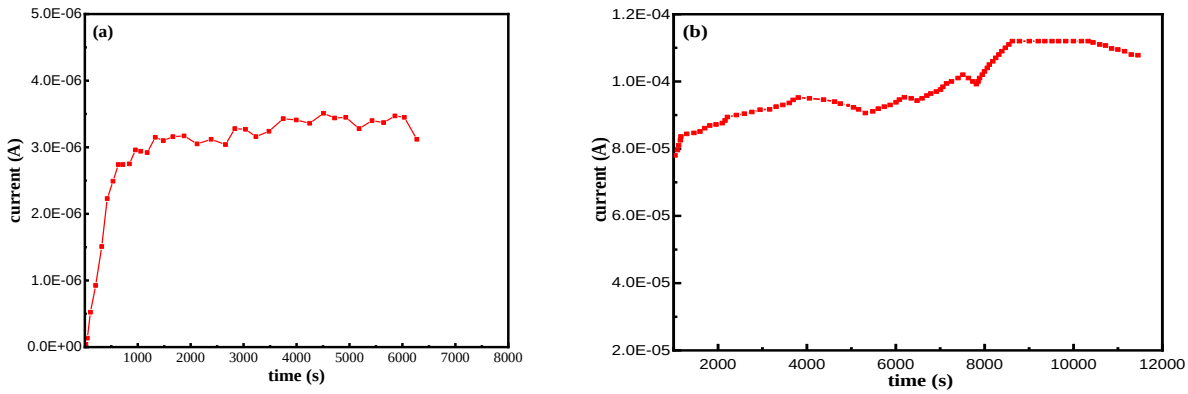

Fig. 5. Hydrogen permeation curves of 316L substrate and coating: (a) substrate, (b) composite coating

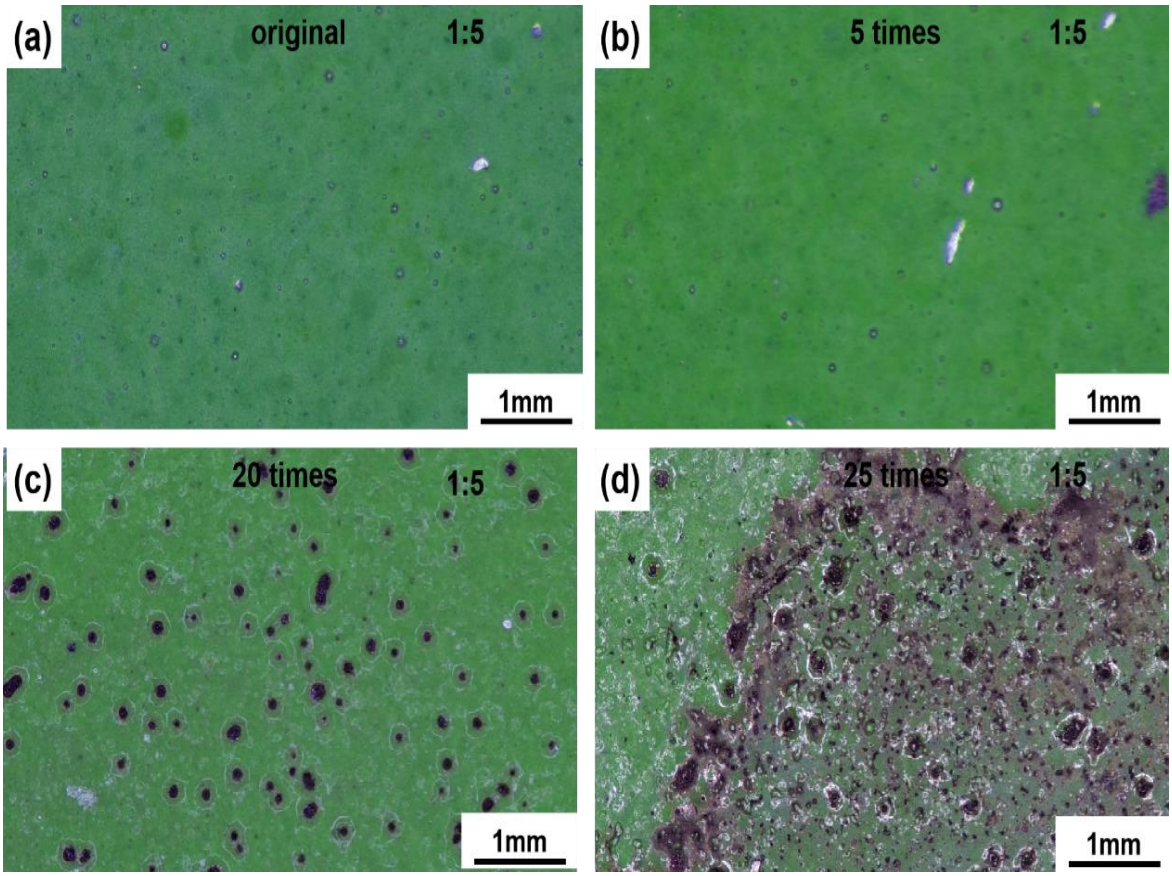

Fig. 6. topography of the coating in different thermal shock times: (a) original, (b) 5times, (c) 20 times, (d) 25times

4. CONCLUSION

At a sintering temperature of 725 °C and a slurry ratio of 1:5, the surface of the composite coating composed of α-Al_2O_3/Cr_2O_3/SiO_2 exhibited smoothness, with a uniform morphology throughout. During the sintering process, chemical reactions led to the formation of phases including α-Al_2O_3, Cr_2O_3, SiO_2, and Al_2SiO_5. The α-Al2O3 was arranged in layered structures, while Cr_2O_3 was evenly distributed within the coating. The permeability resistance factor (PRF) of the coating against hydrogen diffusion relative to the 316L stainless steel substrate reached a value of 15.31. The PRF of the coating against hydrogen diffusion with respect to the 316L substrate reaches 15.31, and the thermal shock resistance of the coating at cracking is 20 times.

DISCLAIMER (ARTIFICIAL INTELLIGENCE)

Author(s) hereby declare that NO generative AI technologies such as Large Language Models (ChatGPT, COPILOT, etc.) and text-to-image generators have been used during the writing or editing of this manuscript.

ACKNOWLEDGEMENTS

This work was supported by the Henan Province basic scientific research fund support project (2022KY11)

COMPETING INTERESTS

Authors have declared that no competing interests exist.

REFERENCES

1. Le PA, Trung VD, Nguyen PL. The current status of hydrogen energy: An overview, RSC advances, 2023;13(40):28262-28287.
2. Gao Hui, Yang Yan, Zhao Xu. Current situation and thinking of hydrogen energy industry development at home and abroad, International Petroleum Economics. 2019; 27(04):9-17.

3. Mueller K, Arlt W, Status and development in hydrogen transport and storage for energy applications, energy technology, 2013;1(9):501-511.
4. Yang N, Deng J, Wang C. High pressure hydrogen leakage diffusion: Research progress, International Journal of Hydrogen Energy; 2023.
5. He D, Lei Y, Zhang C. Deuterium permeation of Al_2O_3/Cr_2O_3 composite film on 316L stainless steel, International Journal of Hydrogen Energy. 2015;40:2899-2903.
6. Dharamshi HK, Bhadeshia H, Prevention of Hydrogen Embrittlement in Steels, ISIJ International. 2016;56:24-36.
7. Zhou QY, Lu ZX, Ling YH. Characteristic and behavior of an electrodeposited chromium (III) oxide/silicon carbide composite coating under hydrogen plasma environment, Fusion Engineering and Design, 2019;143:137-146.
8. Tamura M, Eguchi T, Nanostructured thin films for hydrogen-permeation barrier, Journal of Vacuum Science & Technology A, 2015;33:041503.
9. Zhu L, Zheng L, Xie H. Design and properties of FeAl/Al2O3/TiO2 composite tritium-resistant coating prepared through pack cementation and sol-gel method, Materials Today Communications. 2020;26: 101848.
10. Zheng ZY, Yang ZC, Yan YW, Effects of internal stress and hydrogen penetration on the performance of Er_2O_3 Coatings as Hydrogen Permeation Barriers, ACS Applied Materials & Interfaces. 2024;16:22471-22481.
11. Fowler JD, Chandra D, Elleman TS. Tritium diffusion in Al2O3 and BeO. Journal of the American Ceramic Society. 2007;60(3-4): 155-161.
12. ZHANG T, Zhang Y Q, Wang J Nong. Preparation and hydrogen resistance of 316L stainless steel surface oxide composite coating, Journal of Guangzhou University (Natural Science Edition). 2023; 22(06):69-76.
13. Li Y, Barzagli F, Liu P. Mechanism and evaluation of hydrogen permeation barriers: A Critical Review, Industrial & Engineering Chemistry Research. 2023;62(39):15752-15773.
14. Zhou Chiliou, He Mohan, Xiao Shu. Research progress of hydrogen resistance coating on stainless steel surface, Chemical Industry Progress. 2020;39(09):3458-3468.
15. Liu DG, Yang TT, Liu YL. Thermal shock and tritium resistance of SiO2 coating on the inner wall of 316L stainless steel pipeline, Vacuum. 2021;185:110032.
16. Huang Kezhi. Preparation and hydrogen inhibition mechanism of APTES-GO modified epoxy resin /PVDF organic coating, Beijing General Research Institute of Nonferrous Metals; 2024.
17. Li Junjun, Wang Yunfeng, Zhang Aiju. Effect of metallic aluminum powder and nano-Al_2O_3 powder on the properties of ceramic bond, Chinese Journal of Ceramics. 2021;40(11):3777-3783.

Disclaimer/Publisher's Note: The statements, opinions and data contained in all publications are solely those of the individual author(s) and contributor(s) and not of the publisher and/or the editor(s). This publisher and/or the editor(s) disclaim responsibility for any injury to people or property resulting from any ideas, methods, instructions or products referred to in the content.

© Copyright (2024): Author(s). The licensee is the journal publisher. This is an Open Access article distributed under the terms of the Creative Commons Attribution License (http://creativecommons.org/licenses/by/4.0), which permits unrestricted use, distribution, and reproduction in any medium, provided the original work is properly cited.

Peer-review history:
The peer review history for this paper can be accessed here:
https://www.sdiarticle5.com/review-history/124403